Angular dependence of pump-induced bottomside and topside ionospheric plasma turbulence at EISCAT

M. J. Kosch,[1,2] E. Mjølhus,[3] M. Ashrafi,[4] M. T. Rietveld,[5] T. Yeoman,[6] and S. Nozawa[1]

Received 13 August 2010; revised 14 December 2010; accepted 14 January 2011; published 22 March 2011.

[1] We experimentally observe the location and angular size of the high-frequency (HF) radio window in the bottomside ionosphere, which permits radio wave propagation to the topside ionosphere, with high angular resolution at the European Incoherent Scatter (EISCAT) facility. HF pump-induced ion line enhancements were observed by the EISCAT UHF incoherent scatter radar on the ionospheric bottomside and topside. The radar zenith angle was scanned in small steps in the magnetic meridian. The HF pump duty cycle was deliberately kept low enough to minimize the growth of artificial field-aligned irregularities. The locations of the bottomside radio window and topside enhanced radar echoes are consistent with the expected position determined by ray tracing performed using the observed plasma densities.

Citation: Kosch, M. J., E. Mjølhus, M. Ashrafi, M. T. Rietveld, T. Yeoman, and S. Nozawa (2011), Angular dependence of pump-induced bottomside and topside ionospheric plasma turbulence at EISCAT, *J. Geophys. Res.*, *116*, A03322, doi:10.1029/2010JA016014.

1. Introduction

[2] A high-frequency (HF) radio wave, when transmitted vertically upward with ordinary polarization (O mode) into a horizontally stratified ionosphere, will be reflected downward at the altitude where the electron plasma frequency (f_p) equals the pump wave frequency (f_o), i.e., $X = 1$ where:

$$X = \frac{f_p^2}{f_o^2} \tag{1}$$

For $f_p > f_o$, the O mode wave is evanescent. Still assuming a horizontally stratified ionosphere, this remains true for a range of off-vertical angles of incidence up to the Spitze angle (θ_c), defined as [*Ginzburg*, 1970; *Budden*, 1980]:

$$\sin(\theta_c) = \sin(\alpha)\sqrt{\frac{Y}{1+Y}} \tag{2}$$

$$Y = \frac{f_e}{f_o} \tag{3}$$

where f_e is the electron gyrofrequency (~1.35 MHz at the European Incoherent Scatter (EISCAT) facility F layer) and α is the dip angle of the magnetic field ($\alpha = 12.8°$ at EISCAT). For the F layer at EISCAT, $\theta_c = \sim 5°–6°$, depending on the pump frequency [*Isham et al.*, 1990, 1996]. For radio wave launch directions beyond the Spitze angle θ_c, the radio wave will refract back down for $f_p < f_o$ [e.g., *Budden*, 1985] so that $f_p = f_o$ is not satisfied.

[3] In the high-latitude ionosphere, where α is small, an O mode wave launched at the critical incidence angle θ_c will pass through the radio window [*Budden*, 1980] at the altitude where $X = 1$ without reflection and propagate in the Z mode [*Ginzburg*, 1970; *Mjølhus*, 1990]. Depending on the plasma density profile, upward propagation into denser plasma continues until either the ray is refracted downward, the Z mode reflection altitude is reached (i.e., $X = 1 + Y$), or until the plasma density decreases again (discussed below, see equation (6)) and the topside is reached (i.e., $X = 1$). The Z mode reflection altitude can be approximated by [e.g., *Leyser and Nordblad*, 2009]:

$$f_p \approx f_o + \frac{f_e}{2} \tag{4}$$

The downward propagating Z mode ray continues until the plasma resonance level is reached near the bottomside $X = 1$ altitude, which for small α is given by:

$$X \approx 1 - \sin^2(\alpha)\frac{Y^2}{1-Y^2} \tag{5}$$

The resonance level occurs a small distance below the O mode critical level ($X = 1$), typically <= 0.5 km at EISCAT. According to linear theory, the Z mode wave is converted into an electrostatic Langmuir wave and the energy completely

[1]Solar-Terrestrial Environment Laboratory, Nagoya University, Nagoya, Japan.
[2]On leave from Department of Physics, Lancaster University, Lancaster, UK.
[3]Institute of Mathematical Science, University of Tromsø, Tromsø, Norway.
[4]School of Physics and Astronomy, University of Southampton, Southampton, UK.
[5]EISCAT Research Association, Ramfjordmoen, Norway.
[6]Department of Physics and Astronomy, University of Leicester, Leicester, UK.

0148-0227/11/2010JA016014

dissipated into the plasma [*Golant and Piliya*, 1971; *Mjølhus and Flå*, 1984]. *Gondarenko et al.* [2003] have confirmed this qualitative picture using electromagnetic full wave numerical calculations.

[4] If the ionospheric peak plasma density ($foF2$) satisfies:

$$f_o < foF2 < f_o + \frac{f_e}{2} \tag{6}$$

then the upward propagating Z mode wave will not be refracted or reflected downward and can enter the topside ionosphere. There a similar electrostatic resonance condition as for bottomside ionosphere (i.e., equation (5)) occurs, also with absorption of the wave energy into the plasma [*Mjølhus and Flå*, 1984]. In this case, the plasma resonance altitude is slightly above the $X = 1$ topside altitude. In an ideal perfectly horizontally stratified ionosphere, the Z mode critical ray emanating from the bottomside radio window will also pass exactly through the topside radio window without undergoing electrostatic resonance and continue in the O mode into space. However, since the transmission coefficient of both radio windows is not unity everywhere [*Mjølhus*, 1984], a ring of rays around the Z mode critical ray will undergo partial conversion into electrostatic Langmuir waves on the topside. In addition, as the real ionosphere is never perfectly horizontally stratified because of natural irregularities, gravity waves and tilting, some, possibly all, rays emanating from the bottomside radio window will practically always miss the topside radio window and undergo conversion into electrostatic Langmuir waves on the topside.

[5] Little nonlinear theory exists of what happens when the Z mode wave propagates into the resonance region. However, *Eliasson* [2008] made a numerical two-scale simulation including both bottomside and topside regions. In the bottomside Langmuir turbulence region the study showed generation of Z mode waves which propagate upward. Under condition (6), the Z mode waves propagated to the topside plasma resonance layer, as expected. There the simulation showed that Langmuir cavitation occurred, which might give rise to observable radar echoes. With penetration of the pump waves through the bottomside radio window an even higher energy flux is expected than in the study of *Eliasson* [2008], which relies on secondary generation of Z mode waves. Therefore, even stronger nonlinearity in the topside plasma resonance region should be expected in the present context.

[6] The HF radio window is known to exist because long-delay traces associated with Z mode propagation can sometimes be seen in ionograms. O mode to Z mode conversion in the radio window can be essentially 100% efficient [*Ginzburg*, 1970; *Mjølhus and Flå*, 1984] and therefore a small angular gap in the production of Langmuir waves around θ_c can be expected for the bottomside ionosphere. Maximum transmission through the radio window is in the magnetic meridian plane [*Budden*, 1980], which is ~2° west of the geographic meridian at EISCAT. This small offset is of no practical importance to the results described later. The angular width of the radio window ($\Delta\theta_z$) is a function of the scale length of the plasma density [*Mjølhus*, 1984, 1990]:

$$\Delta\theta_Z = \left[\frac{\pi^2 f_o}{c} L\sqrt{Y}\right]^{-1/2} \tag{7}$$

where $L = (|\nabla n_e|/n_e)^{-1}$ is the scale length of spatial plasma density variation at $X = 1$, c is the speed of light and n_e is the plasma density. Equation (7) gives $\Delta\theta_z < 1°$ at EISCAT for $L \cong 50$ km. A radio window also exists poleward as well as equatorward in the magnetic meridian [*Mjølhus*, 1990], but only the equatorward window will allow the Z mode wave to reach the ionospheric topside. *Mjølhus and Flå* [1984] estimated that topside Z mode reflection would occur ~0.5°–1.5° further south of the equatorward radio window at EISCAT.

[7] Pumping the ionosphere with high-power HF O mode radio waves causes many phenomena to appear. Among these are HF-driven Langmuir turbulence [e.g., *DuBois et al.*, 1993, 2001, and references therein] and field-aligned plasma irregularities (striations) [e.g., *Frolov et al.*, 1997, and references therein]. Near and below the O mode HF reflection altitude ($X = 1$), the radio wave can decay into electron Langmuir and ion acoustic electrostatic waves. At the matching height, where the pump-driven electrostatic waves and observing radar wave vector satisfy the Langmuir dispersion relationship [e.g., *Mjølhus et al.*, 2003, and references therein], strong plasma and ion line backscatter enhancements are routinely observed by VHF and UHF radar systems. The matching height depends on the plasma temperature and radar frequency, typically occurring a few km below $X = 1$ for the EISCAT UHF radar. Pump-induced striations have been known for decades [*Frolov et al.*, 1997]. They are easily stimulated by the thermal parametric instability as a result of resonant mode conversion of the electromagnetic pump wave into upper hybrid (UH) electrostatic waves [*Robinson*, 1989]. Mode conversion occurs efficiently at the upper hybrid resonance height, which is typically a few km below the HF reflection altitude, described by:

$$f_o = f_{UH} = \sqrt{f_p^2 + f_e^2} \tag{8}$$

Pump-induced striations can be readily observed by HF coherent backscatter radars (e.g., SuperDARN) via Bragg scattering provided the backscatter orthogonality condition is met [e.g., *Bond et al.*, 1997; *Robinson et al.*, 1998]. Since striations cause strong anomalous absorption of the HF pump wave [e.g., *Stocker et al.*, 1992; *Robinson*, 2002], their existence is undesirable if plasma resonance experiments near the higher HF reflection altitude are to be performed. One way to mitigate against pump-induced striations is to employ low duty cycle HF pumping with a low average effective radiated power (ERP). In experiments designed to investigate HF pump-driven Langmuir turbulence, *Isham et al.* [1999a, 1999b] used a 2% pump duty cycle of 200 ms on every 10 s with an average ERP of 3.2 MW at EISCAT, *Djuth et al.* [2004] used a 0.33% pump duty cycle of 100 ms on every 30 s with an average ERP of 0.8 MW at EISCAT, and *Sulzer and Fejer* [1994] used a 0.5% pump duty cycle of 5 ms on every 1 s with an average ERP of 0.3 MW at Arecibo. Despite the low average ERP and duty cycle, in all these experiments, the effect of pump-induced striations was evident. Also, performing experiments in the sunlight ionosphere mitigates against F region plasma irregularities because the large E region conductivity is unfavorable for maintaining them [*Djuth et al.*, 2004, and references therein].

[8] The radar manifestation of HF pump-induced Z mode waves above the $X = 1$ bottomside altitude have been

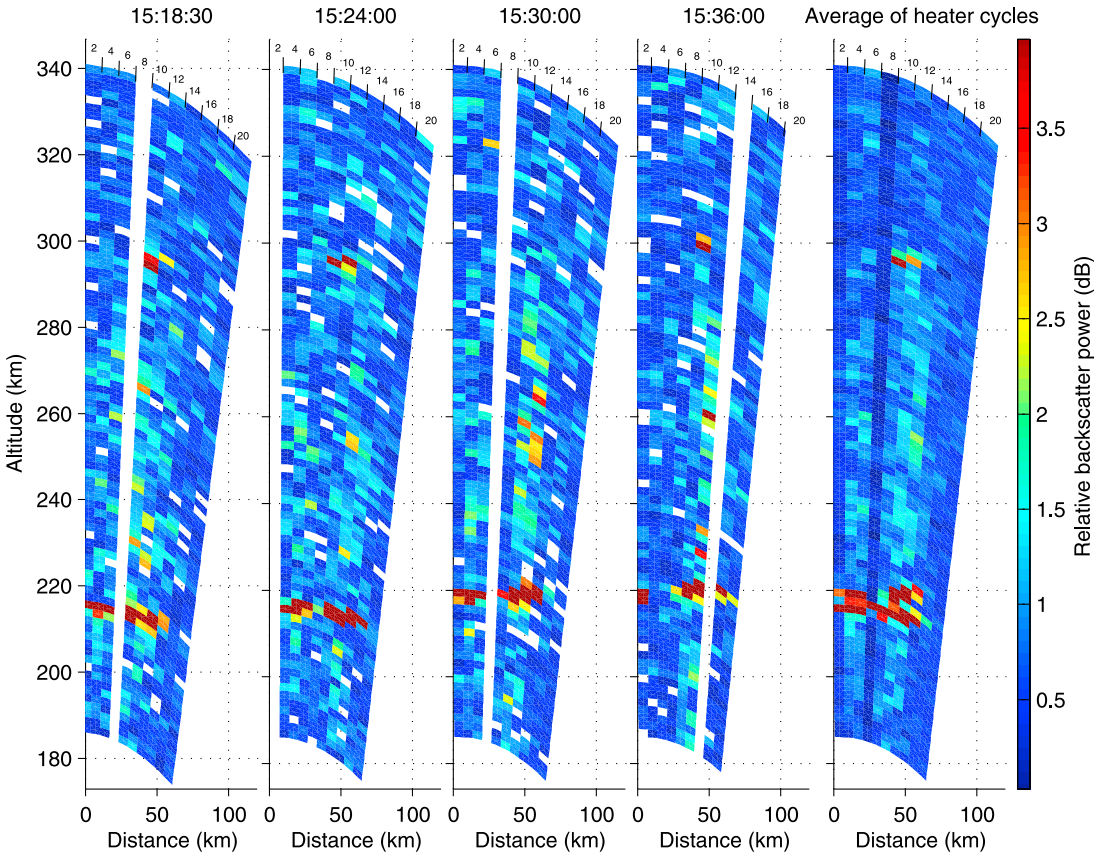

Figure 1a. Relative backscatter power, not corrected for range, as a function of range and angle from 2° to 20° zenith angle south of EISCAT. The range and angular resolution are 1.8 km and 2°, respectively. The first through fourth panels show individual radar scans assembled from 10 HF pump cycles. The fifth panel shows the average of all the available data. Data gaps indicate technical problems with the radar.

observed in situ by rocket [*Gelinas et al.*, 2003] but more frequently by ground-based radar [e.g., *Ganguly and Gordon*, 1983; *Isham et al.*, 1990, 1999a, 1999b] during ionospheric pumping experiments in the *F* region. *Rietveld et al.* [2002] reported similar HF pump-induced radar observations in the *E* region. Using EISCAT radar observations with 2° angular resolution *Isham et al.* [1999a, 1999b] found the topside Z mode signature to occur between the Spitze and magnetic field directions, i.e., ~6° angular width [see *Mishin et al.*, 2001, Figure 2]. The equatorward displacement of the Z mode topside signature relative to θ_c confirmed *Mjølhus and Flå*'s [1984] theoretical estimates. However, the observed ~6° angular width of the Z mode topside signature is much greater than *Mjølhus*'s [1990] theoretical estimate (<1°). *Mishin et al.* [2001] showed that small-scale field-aligned irregularities, either natural or pump induced, could cause the pump-induced Z mode waves to appear for a range of zenith angles and therefore make the apparent radio window widen. Below, we describe observations of the HF radio window at EISCAT while actively monitoring and mitigating against striations.

2. Experiment and Data

[9] The EISCAT facility in Tromsø, northern Norway (69.58°N, 19.23°E), includes two incoherent scatter radars, UHF at 933 MHz and VHF at 224 MHz [*Rishbeth and van Eyken*, 1993], and is colocated with a high-power HF pump facility for artificial heating of the ionospheric plasma operating between 3.85 and 8 MHz [*Rietveld et al.*, 1993].

[10] On 10 June 2004, between 1451 and 1621 UT, the EISCAT HF facility was operated at 4.544 MHz, i.e., between the third and fourth electron gyroharmonic frequency in the F layer, with O mode polarization using an ERP of 106 MW and a cycle of 1 s on every 30 s. The beam was pointing constantly 9° south of vertical. Since the pump beam is ~15° wide, all zenith angles from ~1.5° to 16.5° south are effectively illuminated simultaneously, including the Spitze angle (6.1°), magnetic field line direction (12.8°) and theoretical radio window (launch angle = 6.1°). Geomagnetic conditions were quiet and steady state with the K = 1 at Tromsø and $K_p = 1^-$. The date and time of the experiment ensured that the ionosphere was sunlight and in a near ideal state for a controlled active experiment.

[11] A low 3.3% pump duty cycle with an average ERP of 3.5 MW was used, although subsequent evidence indicates that our ERP estimate should be reduced by ~25% [*Senior et al.*, 2011] to ~2.6 MW. The pumping scheme was an attempt to minimize pump-induced *F* region striations from developing, thereby maintaining as closely as possible the assumption of a smooth horizontally stratified ionosphere while satisfying the need to cover multiple sky positions

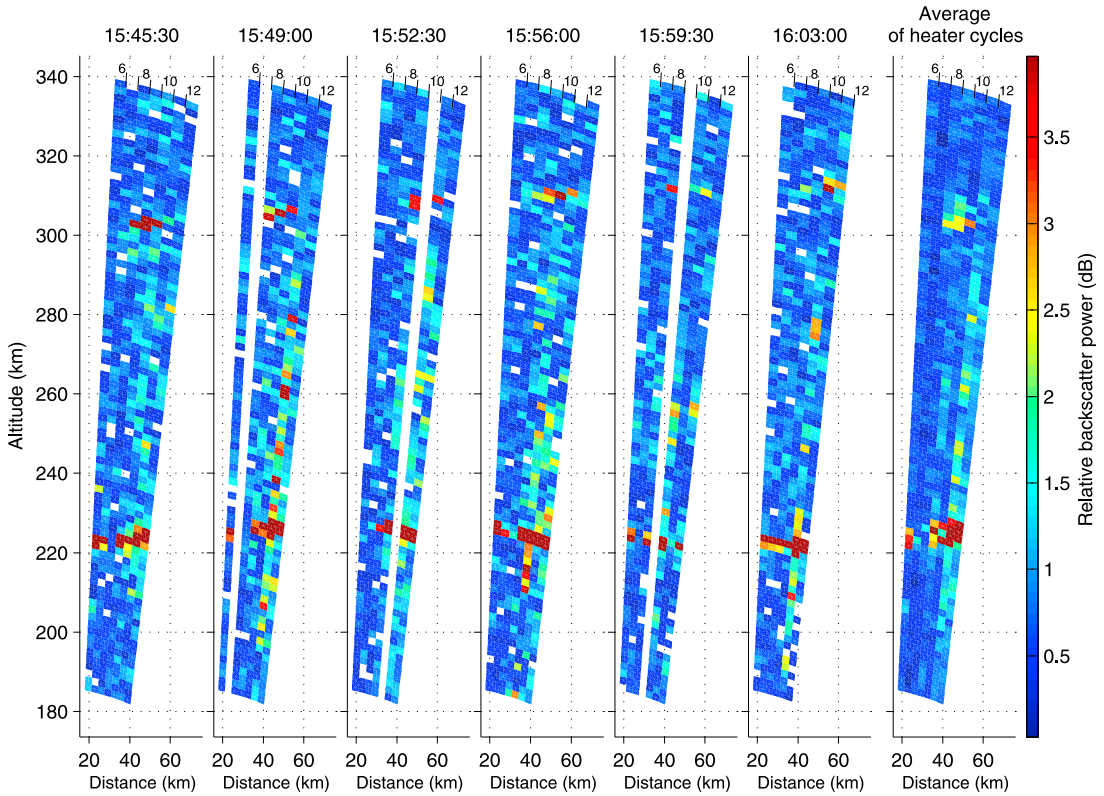

Figure 1b. Relative backscatter power, not corrected for range, as a function of range and angle from 6° to 12° zenith angle south of EISCAT. The range and angular resolution are 1.8 km and 1°, respectively. The first through sixth panels show individual radar scans assembled from 7 HF pump cycles. The seventh panel shows the average of all the available data. Data gaps indicate technical problems with the radar.

repeatedly. The intention was not to cause the Z mode radio window to widen [cf. *Isham et al.*, 1999a, 1999b; *Mishin et al.*, 2001] and to avoid anomalous absorption of the pump wave. Unfortunately for this type of experiment, striations are easily stimulated [e.g., *Djuth et al.*, 2004; *Isham et al.*, 1999a, 1999b; *Sulzer and Fejer*, 1994]. In addition, the possible presence of pump-induced striations was actively monitored using the Hankasalmi SuperDARN HF radar at 11.6 MHz. For this experiment, no striations and therefore no radar backscatter was required. However, the lack of SuperDARN radar backscatter is not a sufficient condition and can also mean that the backscatter orthogonality condition is not met due to HF propagation conditions. Hence, in order to check that the radar would detect striations had they been present, the HF facility was periodically operated with a long pump on pulse of about 1 min in order to create the striations deliberately. In these cases, the Hankasalmi radar did observe strong backscatter (not shown), thereby confirming that the lack of backscatter did indeed mean that our experiment was not creating striations as intended, at least for 11.6 MHz. However, a shortcoming of this method is that only one frequency is monitored and we had no means of monitoring for the presence of plasma irregularities at other scale sizes. Some preconditioning of the ionosphere seems likely given our pump duty cycle and average ERP compared to previous similar experiments [*Djuth et al.*, 2004; *Isham et al.*, 1999a, 1999b; *Sulzer and Fejer*, 1994].

[12] The VHF and UHF radar both recorded ion and plasma line data to monitor the ionospheric plasma density as well as pump-induced backscatter enhancement. Throughout the experiment $foF2$ varied slowly between ~4.6 and ~5.1 MHz; that is, from equation (6) the condition for Z mode propagation at 4.544 MHz to the topside ionosphere was constantly met ($f_oF2 < 4.544 + 1.35/2 = 5.219$ MHz). The VHF radar was using the lti1ov and lti2nv ion and plasma line special program codes, with have intrinsic time resolutions of 20 and 12 ms, respectively. The radar beam pointing was vertically only with range resolutions of 1.5–3.0 km. The UHF radar was using the tau2_pl ion and plasma line alternating code modulation, consisting of a 16-bit alternating code with a bit length of 36 μs. The pulse repetition period was 5.58 ms while the code repeated every 357.12 ms and the data were integrated for 5 s before recording to disk. The receiver sampling interval was 12 μs, corresponding to a range spacing of 1.8 km, but fully independent data points are every 5.4 km. Power profiles of downshifted plasma lines in 8 filter bands, each ±42 kHz wide, were also measured between 167 and 470 km (fully decoded). The beam pointing direction was altered every 30 s in the north-south geographic meridian, which is a close approximation to the geomagnetic meridian. The UHF radar was synchronized to the pump cycle, so that a two-dimensional spatial view of pump-induced backscatter could be created. The experiment proceeded in three different phases, marked by the angular range and step size

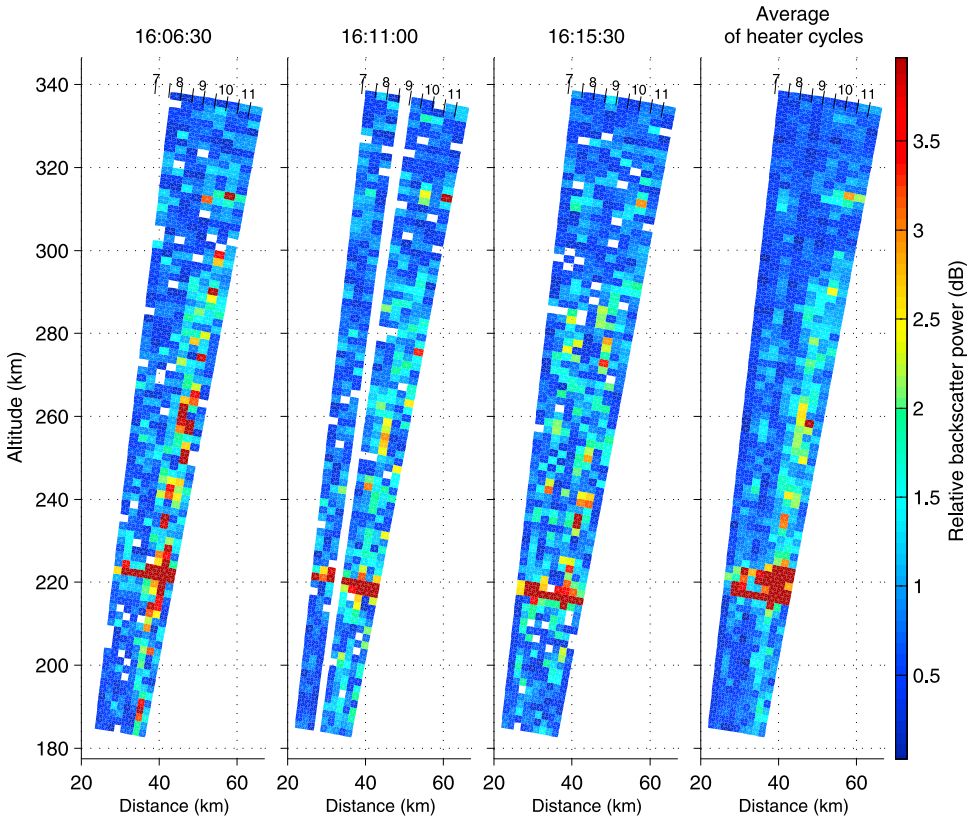

Figure 1c. Relative backscatter power, not corrected for range, as a function of range and angle from 7.5° to 11.5° zenith angle south of EISCAT. The range and angular resolution are 1.8 km and 0.5°, respectively. The first through third panels show individual radar scans assembled from 9 HF pump cycles. The fourth panel shows the average of all the available data. Data gaps indicate technical problems with the radar.

of the UHF radar pointing direction. Both the VHF and UHF radars observed pump-induced ion line enhancements and intermittently plasma line enhancements. Here we present only the UHF ion line data in detail for the equatorward radio window.

[13] Figure 1a shows UHF radar raw backscatter power in the F layer for zenith angles from 2° to 20° south in steps of 2°. Technical problems with the UHF radar resulted in some data gaps, which are easily seen. There are 4 complete cycles between 1518:00 and 1541:00 UT. The pump-induced enhanced backscatter is seen between ~210 and 220 km altitude (red) from 2° to 16° zenith angle. This is the normal O mode signature of pump-induced Langmuir turbulence. Enhanced backscatter is also seen between ~295 and 300 km altitude for ~10°–12° zenith angle in 3 of the 4 scans (not 1530 UT). This is the signature of the Z mode wave approaching resonance on the ionospheric topside. Apparent also is an angular gap in the bottomside backscatter in 2 of the 4 scans, corresponding to the radio window. For 1524:00 UT this occurs at 10° and 1536:00 UT at 4°–6° south. Unfortunately, UHF radar data gaps for the other scans seemingly occur just for the direction where the angular gap in backscatter might have occurred. The fifth panel in Figure 1a shows the average of the 4 individual scans. Here it is clear that the topside enhanced backscatter does not correspond exactly to the angular gap in bottomside enhanced backscatter, rather it occurs at ~2°–4° further south.

[14] Figure 1b is in the same format as Figure 1a except the zenith angles of the scan range from 6° to 12° in 1° steps. There are 6 complete cycles between 1545:30 and 1606:30 UT. Here the pump-induced bottomside and topside backscatter enhancements are seen at ~220–225 and ~300–310 km altitude. The morphology is similar to that of Figure 1a. The average of all scans is shown in the seventh panel in Figure 1b. The radio window can be seen as a gap in the bottomside enhanced backscatter for 4 of the scans and is obvious in the average of all scans for 7°–8° south. The topside enhanced backscatter is seen in all scans, initially 8°–10° south for the first 2 scans and then shifting further equatorward in the later scans, up to 10°–12° south for the last scan. From the average of all the scans, the angular width of the radio window is ~2° and of the topside enhanced backscatter is ~3°. The equatorward displacement of the topside enhanced backscatter is ~1°–2° relative to the radio window.

[15] The UHF radar beam is ~0.6° wide, which limits the smallest useful angular step size. Figure 1c is in the same format as Figures 1a and 1b except the zenith angles of the scan range from 7.5° to 11.5° in 0.5° steps. There are 3 complete cycles between 1606:30 and 1620:00 UT. The bottomside and topside enhanced backscatter occurs for ~215–225 and ~310–315 km altitude, respectively. Unfortunately, ionospheric conditions appeared to be less favorable, so the radio window is not clearly apparent and topside enhanced backscatter ill defined.

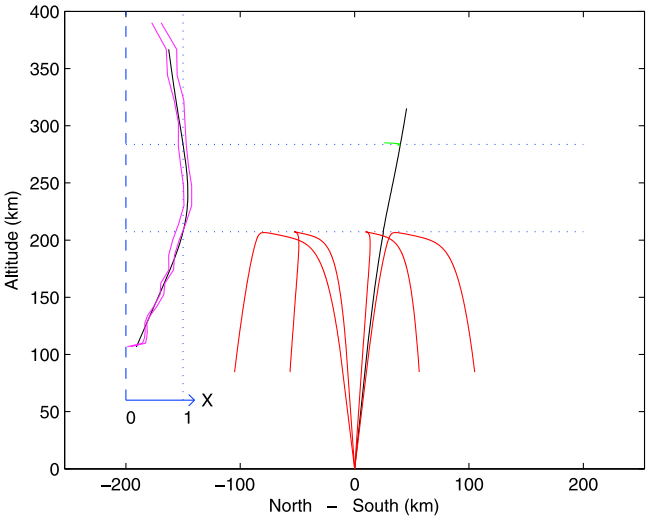

Figure 2a. Ray trace of O mode waves (red) in the magnetic meridian for ±4° and ±7° launch angles and penetrating Z mode wave (black) at 6.1° S launch angle corresponding to Figure 1a. The topside electrostatic wave (green) is shown for the first 10 ms of its existence. The inset curves indicate the average plasma density data from 1528 to 1531 UT with measurement uncertainty (magenta) and analytical profile used for ray tracing (black). The horizontal dashed lines (blue) indicate the heights where the plasma and pump frequencies are equal.

[16] A colocated HF sounder, a Dynasonde [*Rietveld et al.*, 2008], made swept frequency soundings every 2 min between 1 and 10 MHz during the experiment. In about half of the ionograms made during the experiment reported here, clear Z mode traces from the *F* region were visible, showing independently that the radio window was present.

3. Results and Discussion

[17] Figures 2a–2c show ray tracing of the pump wave based on EISCAT data (shown in inset), assuming f_e = 1.35 MHz and α = 12.8°. Figures 2a–2c are for density profiles averaged over 1528–1531, 1555–1558 and 1615–1618 UT, shown as the magenta curves separated by the measurement uncertainty, and correspond to Figures 1a–1c, respectively. To facilitate the ray tracing, the density profiles have been used to fit a function (black curve), which permits analytical differentiation. The fit ensures that the peak plasma density has the observed value at the observed altitude as this has the greatest impact on ray propagation. The horizontal blue dashed lines indicate the critical altitude where $X = 1$ ($f_p = f_o = 4.544$ MHz). The model bottomside (topside) critical levels are 207.3 (283.7), 220.4 (300.5) and 212.8 (316.9) km for Figures 2a–2c, respectively, and correspond approximately (though not exactly) to the enhanced radar backscatter seen in Figures 1a–1c, respectively. The O mode wave propagation is shown in red for launch angles of ±4° and ±7° relative to vertical. The critical O mode ray, which transforms into Z mode at the bottomside radio window, is shown in black for a launch angle of 6.1°. This angle is known precisely for the ideal horizontally stratified ionosphere. Propagation of the critical ray follows the O mode

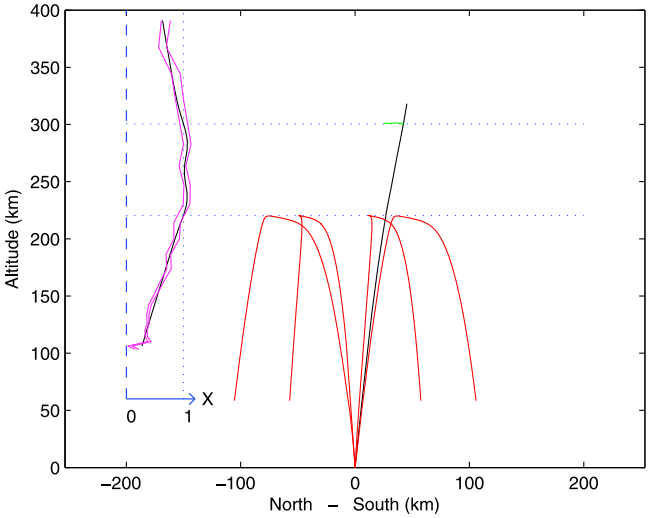

Figure 2b. Same as Figure 2a except corresponding to Figure 1b. The plasma density data are from 1555 to 1558 UT.

and Z mode dispersion relationship for altitudes below and above $X = 1$, respectively, in the bottomside ionosphere. The green ray represents the first ~10 ms of propagation beyond the topside $X = 1$ level, assuming that the inverse radio window is not found. In this phase, the Z mode wave becomes increasingly electrostatically, i.e., longitudinally, polarized and the index of refraction increases to values larger than 1. When the wave approaches the plasma resonance level and beyond, it becomes a Langmuir wave. The wave vector is essentially vertical but the group velocity is nearly perpendicular to the wave vector in this phase, so that the ray moves nearly horizontally. It is expected that this wave will be fully absorbed into plasma within 10 ms. Further details of the ray trace can be found in Appendix A.

[18] From the ray trace, the location of the bottomside (topside) resonant volume is at 7.0° (8.2), 7.0° (8.1) and

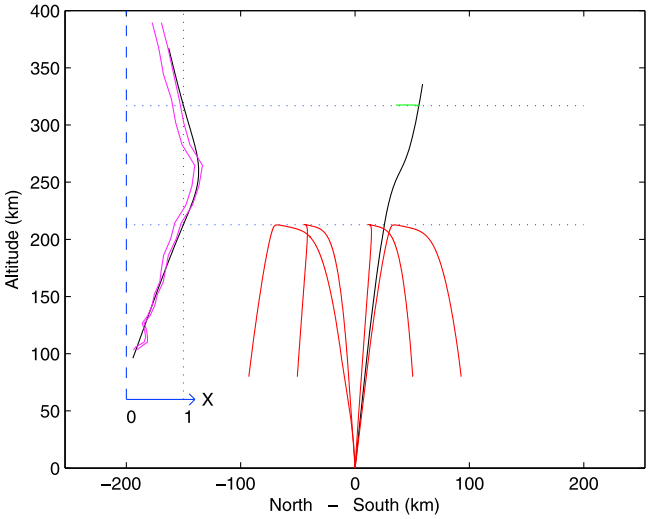

Figure 2c. Same as Figure 2a except corresponding to Figure 1c. The plasma density data are from 1615 to 1618 UT.

6.9° (10.0) south of vertical for Figures 2a–2c, respectively. Figure 1b shows the bottomside radio window most clearly, located on average at 7°–8° south. This is slightly further equatorward than expected. Figures 1a and 1b show the average topside enhanced radar backscatter most clearly, located at 10°–12° and 8°–10° south. Again, our observations are slightly equatorward of the expected position. However, the equatorward displacement of the topside echo relative to the bottomside radio window is consistent with the theoretical expectation [*Mjølhus and Flå*, 1984] and according to our ray calculations. Shifting the radio window and topside echo equatorward by ~1° further south can be achieved by tilting the ionosphere by ~2° such that the plasma density at a fixed altitude increases toward the south, which seems entirely feasible [e.g., *Nygrén et al.*, 1997; *Tereshchenko et al.*, 2000]. Indeed, there is supporting evidence from a colocated HF sounder for such a tilt. The ionogram inversion program "NeXtYZ" reconstructs an electron density profile allowing for a horizontal gradients and tilts as described in more detail by *Zabotin et al.* [2006]. A wedge-stratified ionospheric model is used instead of the traditional plane-stratified ionosphere. The ionospheric echoes obtained from the Dynasonde contain direction of arrival information which is necessary input to constrain the variation of local three-dimensional tilts of ionospheric layers with height in the inversion. Averaging the 213 north-south tilts obtained between 1450 and 1622 UT in the real height interval 200 to 230 km, which corresponds approximately to the height interval most likely to affect the propagation of the 4.544 MHz pump wave, gives a mean southward tilt of 1.6° with a standard deviation of 4.0°. The standard deviation probably reflects the variability of the tilted ionosphere.

[19] From the measured density profiles we have derived the bottomside scale heights L = 199, 146 and 119 km, and applying equation (7) we obtain radio window angular widths of $\Delta\theta_z$ = 0.45°, 0.52° and 0.58° for Figures 2a–2c, respectively. This is in reasonable agreement with our observation of 2° from Figures 1a and 1b. It is not surprising that the ideal is narrower than the observed radio window as the ionosphere will never be perfectly smooth or horizontally stratified [cf. *Mishin et al.*, 2001], possibly due to some HF pump preconditioning. This emphasizes the importance of finding an undisturbed ionosphere and maintaining a low pump duty cycle in order to successfully execute our experiment.

[20] We note that there is presently no theoretical expectation as to the nature of the source of the radar echoes from the Z mode driven plasma resonance region, both for the bottomside and topside ionosphere. For linear theory, the electrostatically polarized (Langmuir) wave does not have sufficient lifetime relative to collisional dissipation to propagate to a state where its wave number would be observable by the EISCAT UHF radar. However, the local energy flux is large enough that a very high energy density is expected in the resonance region, where the group velocity is small, and therefore a strongly nonlinear process is expected [*Mjølhus and Flå*, 1984].

4. Conclusion

[21] We have observed the radar manifestation of the Z mode ionospheric radio window with high angular resolution in the equatorward meridian using the EISCAT HF pump facility and UHF radar for comparison with theoretical predictions. Ionospheric bottomside and topside enhanced ion line radar echoes were observed with a 3.3% HF pump duty cycle and an average ERP of <3.5 MW. Active monitoring by HF radar showed that no observable pump-induced striations were generated at 11.6 MHz. The equatorward radio window has an angular width of 2°, most often appearing 7°–8° south. This corresponds to the topside echo of 2°–3° angular width displaced 8°–12° south. HF ray tracing of the pump wave, using an analytical representation of the observed plasma density profile, is consistent with the observations, especially if an ionospheric tilt of ~2° is included for which there is supporting evidence from a colocated HF sounder.

Appendix A

[22] The general equations for ray tracings calculations are:

$$\begin{aligned} \frac{d\mathbf{x}}{dt} &= \frac{\partial\omega}{\partial\mathbf{k}} \\ \frac{d\mathbf{k}}{dt} &= -\frac{\partial\omega}{\partial\mathbf{x}} \end{aligned} \tag{A1}$$

where $\mathbf{x}$ is the position vector of the "wave particle," $\mathbf{k}$ its wave vector, and the function $\omega(\mathbf{k}, \mathbf{x})$ defines the dispersion relation giving the frequency ω as function of $\mathbf{k}$ and $\mathbf{x}$, where the $\mathbf{x}$ dependence is due to inhomogeneity of the medium. For a cold magnetized plasma it is impractical to solve for ω this way. Hence, the Booker quartic [e.g., *Mjølhus and Flå*, 1984] is used in combination with implicit differentiation, to obtain the following set of differential equations for a ray in the magnetic meridian plane:

$$\begin{aligned} \frac{dz}{ds} &= \frac{\partial B}{\partial n_z} \\ \frac{dy}{ds} &= \frac{\partial B}{\partial n_y} \\ \frac{dn_z}{ds} &= -\frac{\partial B}{\partial X}\frac{dX}{dz} \\ \frac{dn_y}{ds} &= 0 \end{aligned} \tag{A2}$$

where z and y are the vertical and horizontal coordinates, respectively, $X(z)$ describes the variation of the plasma density, assuming horizontal stratification, and $n_{y,z}$ are the normalized components of the wave vector $(n_y, n_z) = (c/\omega)(k_y, k_z)$. The dispersion relation has the form:

$$B(X, Y, \alpha, n_y, n_z) = 0 \tag{A3}$$

where B is the Booker quartic, having the form:

$$B = \varepsilon_{zz} n_z^4 + a n_z^3 + b n_z^2 + c n_z + d \tag{A4}$$

The coefficients in (A4) will not be given here, except:

$$\varepsilon_{zz} = 1 - \frac{X}{1 - Y^2}\left(1 - Y^2 \cos^2\alpha\right) \tag{A5}$$

For the other coefficients, the reader is referred to *Mjølhus and Flå* [1984], where expressions for them can be found. Finally, the relation between the auxiliary parameter s and time t is given by:

$$\frac{dt}{ds} = -\frac{\omega}{c}\frac{\partial B}{\partial \omega} \tag{A6}$$

The ray that hits the radio window has the (constant) value $n_y = n_{yc}$, where:

$$n_{yc} = \sqrt{\frac{Y}{1+Y}}\sin\alpha \tag{A7}$$

We have calculated such rays in three cases, based on measured values of the plasma density. The measured density profiles were approximated by smooth analytical functions which will not be further described here but which are shown in the insets of Figures 2a–2c together with bounds of the measured densities. The calculations were in each case started at heights slightly above 100 km, assuming the ray to be unrefracted below this level.

[23] The radio window manifests itself as a saddle point for the system (A2) which the critical ray satisfying $n_y = n_{yc}$ approaches; see *Mjølhus and Flå* [1984] and *Mjølhus* [1984] for details on this saddle point structure. The ray computation is carried past the radio window by stopping the calculation when it comes sufficiently near, then continuing on the other side of the saddle point. In order to continue, the sense of variation of the parameter s must be reversed. In our calculation, the stopping criterion was given by $1 - X = \varepsilon$ with $\varepsilon = 0.005$. Then it was checked that the trajectory was near the invariant direction toward the saddle point (i.e., the stable manifold), and then a starting point on the invariant curve in (X, n_z) space on the other side of the saddle point was calculated and the integration continued. The integration then proceeded to the topside, where the ray represents a wave propagating in the Z mode, until the level $X = 1$ was again reached. There, a similar procedure was performed, and the ray was continued to $X < 1$ representing an O mode wave.

[24] A ray which approaches the topside level $X = 1$ from below in the Z mode, while not satisfying $n_y = n_{yc}$ perfectly, will not pass the radio window but will instead continue toward the plasma resonance:

$$\varepsilon_{zz} = 0 \tag{A8}$$

(and beyond when warm plasma extension is included). Along this path n_z will increase and the wave will become gradually more electrostatically polarized. The green rays seen in Figures 2a–2c represent the latter process. In order to do this calculation, the Booker quartic was extended with a thermal correction:

$$\begin{gathered}\varepsilon_{zz} \mapsto \varepsilon_{zz} - \beta n_z^2 \\ \beta = 3(v_{th}/c)^2\end{gathered} \tag{A9}$$

where v_{th} is the electron thermal velocity [e.g., *Mjølhus and Flå*, 1984]. The ray was started from the topside $X = 1$ level and continued until a stopping criterion was reached. This stopping criterion was defined in terms of an assumed life time of the Langmuir wave. It can be shown [*Dysthe et al.*, 1980] that the propagation time of a Langmuir wave, until n_z has achieved a certain (large) value, is:

$$T \sim 2\frac{L}{c}n_z. \tag{A10}$$

The lifetime of the electrostatic wave is determined by collisional damping [*Dysthe et al.*, 1980]. By selecting a value of T accordingly, a maximal value of n_z for a stopping criterion can be determined. In our calculations $T = 10$ ms was used. The ray so obtained goes nearly perpendicular to the density gradient, i.e., nearly perpendicular to its wave vector. This is characteristic for electrostatic waves having a wave vector oblique to the magnetic field.

[25] **Acknowledgments.** EISCAT is an international research association supported by research organizations in China (CRIRP), Finland (SA), Germany (DFG), Japan (NIPR and STEL), Norway (NFR), Sweden (VR), and the United Kingdom (STFC). M.J.K. acknowledges funding support for his visiting professorship from the Solar-Terrestrial Environment Laboratory of Nagoya University. Brett Isham developed the lti1ov and lti2nv VHF radar codes. Vasyl Belyey operated the VHF radar and analyzed the data.

[26] Robert Lysak thanks Brett Isham and Evgeny Mishin for their assistance in evaluating this paper.

References

Bond, G. E., et al. (1997), Spatial observations by the CUTLASS coherent scatter radar of ionospheric modification by high power radio waves, *Ann. Geophys.*, *15*, 1412–1421, doi:10.1007/s00585-997-1412-4.

Budden, K. G. (1980), The theory of radio windows in the ionosphere and magnetosphere, *J. Atmos. Terr. Phys.*, *42*, 287–298, doi:10.1016/0021-9169(80)90036-7.

Budden, K. G. (1985), *The Propagation of Radio Waves*, doi:10.1017/CBO9780511564321, Cambridge Univ. Press, New York.

Djuth, F. T., B. Isham, M. T. Rietveld, T. Hagfors, and C. La Hoz (2004), First 100 ms of HF modification at Tromsø, Norway, *J. Geophys. Res.*, *109*, A11307, doi:10.1029/2003JA010236.

DuBois, D. F., A. Hanssen, H. A. Rose, and D. Russell (1993), Space and time distribution of HF excited Langmuir turbulence in the ionosphere: Comparison of theory and experiment, *J. Geophys. Res.*, *98*, 17,543–17,567, doi:10.1029/93JA01469.

DuBois, D. F., et al. (2001), High-power high-frequency-induced Langmuir turbulence in the smooth ionosphere at Arecibo. I. Theoretical predictions for altitude-resolved plasma line spectra, *Phys. Plasmas*, *8*, 791–801, doi:10.1063/1.1345703.

Dysthe, K. B., et al. (1980), Nonlinear mixing in the ionosphere, *Phys. Scr.*, *21*, 122–128, doi:10.1088/0031-8949/21/1/016.

Eliasson, B. (2008), Full-scale simulation study of the generation of topside ionospheric turbulence using a generalized Zakharov model, *Geophys. Res. Lett.*, *35*, L11104, doi:10.1029/2008GL033866.

Frolov, V. L., et al. (1997), Temporal behaviour of artificial small-scale ionospheric irregularities: Review of experimental results, *J. Atmos. Sol. Terr. Phys.*, *59*, 2317–2333, doi:10.1016/S1364-6826(96)00126-5.

Ganguly, S., and W. E. Gordon (1983), Heater enhanced topside plasma line, *Geophys. Res. Lett.*, *10*, 977–978, doi:10.1029/GL010i010p00977.

Gelinas, L. J., M. C. Kelley, M. P. Sulzer, E. Mishin, and M. J. Starks (2003), In situ observations during an HF heating experiment at Arecibo: Evidence for Z-mode and electron cyclotron harmonic effects, *J. Geophys. Res.*, *108*(A10), 1382, doi:10.1029/2003JA009922.

Ginzburg, V. L. (1970), *The Propagation of Electromagnetic Radio Waves in Plasmas*, 2nd ed., Pergamon, New York.

Golant, V. E., and A. D. Piliya (1971), Linear transformation of waves in a plasma, *Usp. Fiz. Nauk.*, *104*, 413–457. (*Sov. Phys. Usp., Engl. Transl.*, *14*, 413–437, 1972.)

Gondarenko, N. A., P. N. Guzdar, S. L. Ossakow, and P. A. Bernhardt (2003), Linear mode conversion in inhomogeneous magnetized plasmas during ionospheric modification by HF radio waves, *J. Geophys. Res.*, *108*(A12), 1470, doi:10.1029/2003JA009985.

Isham, B., W. Kofman, T. Hagfors, J. Nordling, B. Thidé, C. LaHoz, and P. Stubbe (1990), New phenomena observed by EISCAT during an RF ionospheric modification experiment, *Radio Sci.*, *25*, 251–262, doi:10.1029/RS025i003p00251.

Isham, B., et al. (1996), Recent EISCAT heating results using chirped ISR, *J. Atmos. Terr. Phys.*, *58*, 369–383, doi:10.1016/0021-9169(95)00042-9.

Isham, B., et al. (1999a), Aspect angle dependence of HF enhanced incoherent backscatter, *Adv. Space Res.*, *24*, 1003–1006, doi:10.1016/S0273-1177(99)00555-4.

Isham, B., et al. (1999b), A search for the location of the HF excitation of enhanced ion acoustic and Langmuir waves with EISCAT and the Tromsø heater, *Radiophys. Quantum Electron.*, *42*, 533–543, doi:10.1007/BF02677559.

Leyser, T. B., and E. Nordblad (2009), Self-focused radio frequency L wave pumping of localised upper hybrid oscillations in the high-latitude ionospheric plasma, *Geophys. Res. Lett.*, *36*, L24105, doi:10.1029/2009GL041438.

Mishin, E., T. Hagfors, and B. Isham (2001), A generation mechanism for topside enhanced incoherent scatter backscatter during high frequency modification experiments in Tromsø, *Geophys. Res. Lett.*, *28*, 479–482, doi:10.1029/2000GL000122.

Mjølhus, E. (1984), Coupling of Z mode near critical angle, *J. Plasma Phys.*, *31*, 7–28, doi:10.1017/S0022377800001392.

Mjølhus, E. (1990), On linear conversion in a magnetized plasma, *Radio Sci.*, *25*, 1321–1339, doi:10.1029/RS025i006p01321.

Mjølhus, E., and T. Flå (1984), Direct access to plasma resonance in ionospheric radio experiments, *J. Geophys. Res.*, *89*, 3921–3928, doi:10.1029/JA089iA06p03921.

Mjølhus, E., et al. (2003), Geometric aspects of HF driven Langmuir turbulence in the ionosphere, *Nonlinear Processes Geophys.*, *10*, 151–177, doi:10.5194/npg-10-151-2003.

Nygrén, T., et al. (1997), Comparison of the *F* region electron density observations by satellite radio tomography and incoherent scatter methods, *Ann. Geophys.*, *14*, 1422–1428.

Rietveld, M. T., et al. (1993), Introduction to ionospheric heating at Tromsø I—Experimental overview, *J. Atmos. Terr. Phys.*, *55*, 577–599, doi:10.1016/0021-9169(93)90007-L.

Rietveld, M. T., et al. (2002), HF-pump-induced parametric instabilities in the auroral *E* region, *Adv. Space Res.*, *29*, 1363–1368, doi:10.1016/S0273-1177(02)00186-2.

Rietveld, M. T., et al. (2008), The Tromsø Dynasonde, *Polar Sci.*, *2*(1), 55–71, doi:10.1016/j.polar.2008.02.001.

Rishbeth, H., and A. P. van Eyken (1993), EISCAT: Early history and the first ten years of operation, *J. Atmos. Terr. Phys.*, *55*, 525–542, doi:10.1016/0021-9169(93)90002-G.

Robinson, T. R. (1989), The heating of the high latitude ionosphere by high power radio waves, *Phys. Rep.*, *179*, 79–209, doi:10.1016/0370-1573(89)90005-7.

Robinson, T. R. (2002), Effects of multiple scatter on the propagation and absorption of electromagnetic waves in a field-aligned-stratified cold magneto-plasma: Implications for ionospheric modification experiments, *Ann. Geophys.*, *20*, 41–55, doi:10.5194/angeo-20-41-2002.

Robinson, T. R., et al. (1998), First CUTLASS-EISCAT heating results, *Adv. Space Res.*, *21*, 663–666, doi:10.1016/S0273-1177(97)01000-4.

Senior, A., M. T. Rietveld, W. Singer, F. Honary, and M. J. Kosch (2011), Measurements and modeling of cosmic noise absorption changes due to radio heating of the D region ionosphere, *J. Geophys. Res.*, doi:10.1029/2010JA016189, in press.

Stocker, A. J., T. R. Robinson, and T. B. Jones (1992), Observations of the effects of ionospheric heating on the amplitude of low-power diagnostic radio waves at Arecibo, *J. Geophys. Res.*, *97*, 6315–6322, doi:10.1029/92JA00146.

Sulzer, M. P., and J. A. Fejer (1994), Radar spectral observations of HF-induced ionospheric Langmuir turbulence with improved range and time resolution, *J. Geophys. Res.*, *99*, 15,035–15,050, doi:10.1029/94JA00673.

Tereshchenko, E. D., et al. (2000), Irregular structures of the F layer at high latitudes during ionospheric heating, *Ann. Geophys.*, *18*, 1197–1209, doi:10.1007/s00585-000-1197-1.

Zabotin, N. A., J. W. Wright, and G. A. Zhbankov (2006), NeXtYZ: Three-dimensional electron density inversion for dynasonde ionograms, *Radio Sci.*, *41*, RS6S32, doi:10.1029/2005RS003352.

M. Ashrafi, School of Physics and Astronomy, University of Southampton, Southampton SO17 1BJ, UK.

M. J. Kosch and S. Nozawa, Solar-Terrestrial Environment Laboratory, Nagoya University, Nagoya 464-8601, Japan. (m.kosch@lancaster.ac.uk)

E. Mjølhus, Institute of Mathematical Science, University of Tromsø, N-9037 Tromsø, Norway.

M. T. Rietveld, EISCAT Research Association, N-9027 Ramfjordmoen, Norway.

T. Yeoman, Department of Physics and Astronomy, University of Leicester, Leicester LE1 7RH, UK.